Detection of body position changes using the surface electrocardiogram

M. Åström[1] J. García[2] P. Laguna[2] O. Pahlm[3] L. Sörnmo[1]

[1]Signal Processing Group, Department of Electroscience, Lund University, Lund, Sweden
[2]Grupo de Tecnologías de las Comunicaciones, Aragon Institute for Engineering Research (IZA), Universidad de Zaragoza, Zaragoza, Spain
[3]Department of Clinical Physiology, Lund University, Lund, Sweden

Abstract—*A method for detecting body position changes that uses the surface vectorcardiogram (VCG) is presented. Such changes are often manifested as sudden shifts in the electrical axis of the heart and can erroneously be interpreted as acute ischaemic events. Axis shifts were detected by analysing the rotation angles obtained from the alignment of successive VCG loops to a reference loop. Following the rejection of angles originating from noise events, the detection of body position changes was performed on the angle series using a Bayesian approach. On a database of ECG recordings from normal subjects performing a predefined sequence of body position changes, a detection rate of 92% and a false alarm rate of 7% was achieved.*

Keywords—*Body position, Ischaemia monitoring, Loop alignment, Rotation angles, VCG loops*

Med. Biol. Eng. Comput., 2003, **41**, 164–171

1 Introduction

MYOCARDIAL ISCHAEMIA is manifested in the ECG as a change in the ST-T segment, sometimes accompanied by a change in QRS morphology during the advanced stages of ischaemia. Unfortunately, a change in body position also affects the QRS complex and the ST-T segment and can be misclassified as an acute ischaemic event by the monitoring equipment used in the intensive care unit. Therefore it would be highly desirable to introduce a means for reducing the number of false alarms or, at least, to inform the staff whether or not a detected event is a likely body position change (BPC).

Several recent studies have documented the effect of BPCs on the ECG/VCG; these studies are descriptive in nature and quantify the effect on various types of ECG measurement. In one study, the standard 12-lead ECG and the derived 12-lead ECG (using the so-called Dower's EASI lead system) were compared in terms of QRS and ST-T changes for different body positions (ADAMS and DREW, 1997). It was concluded that BPCs influence all ECG measurements to various degrees, although those related to the QRS morphology are more sensitive than those related to the ST-T segment. Another paper investigated the types of QRS and ST-T change that accompany a BPC and reported that the effects on the ST-T segment were usually small (JERNBERG *et al.*, 1997). Yet another paper has dealt with BPCs in relation to ischaemia monitoring: changes in the VCG were studied in terms of vector differences of the QRS complex and vector magnitude changes of the ST-T segment (NØRGAARD *et al.*, 2000); see also JENSEN *et al.* (1997). The results showed that both types of measurement are rather sensitive to BPCs, especially during changes to the left lateral position. It was concluded that monitoring algorithms have a limited value unless they are combined with BPC detection (NØRGAARD *et al.*, 2000).

It was recently suggested that different positional ECG templates should be recorded at the onset of ischaemia monitoring for later use in the software discriminating between transient myocardial ischaemia and BPCs (DREW and ADAMS, 2001). This idea will probably help in reducing the number of falsely detected ischaemic events. However, as also correctly pointed out by the authors, the initial learning procedure is not very feasible in unstable patients.

Although the undesirable effect of a BPC is well-established in ischaemia monitoring, ECG-based methods developed for alleviating this problem have been rare. One of the few studies addressing this problem was presented by Jager and colleagues (JAGER *et al.*, 1998), who made use of the Karhunen–Loève transform for detecting ischaemic ST-T changes as well as non-ischaemic episodes due to BPCs. They developed an algorithm that analyses the trajectory of the transform coefficients of successive QRST intervals, under the hypothesis that a BPC is associated with an abrupt trajectory change, whereas an ischaemic episode is manifested by a much more gradual change. In a recent study, Nelwan and colleagues developed a new technique for detecting BPCs, based on both scalar and spatial measurements; the technique was found to be useful for reducing the number of false alarms in an automated monitoring system (NELWAN *et al.*, 2000).

Another approach to BPC detection is to use a set of sensors that produce a voltage proportional to the acceleration associated with different body movements. Such measurement systems have recently received considerable attention for the purpose of monitoring body posture and motion (FOERSTER *et al.*, 1999;

Correspondence should be addressed to Professor Leif Sornmo; email: leif.sornmo@es.lth.se

Paper received 24 June 2002 and in final form 31 October 2002
MBEC online number: 20033749

AMINIAM *et al.*, 1999; NG *et al.*, 2000). Although such an approach offers an exact, objective description of body movements, the extra sensors needed and related recording equipment make the approach less useful in intensive care monitoring.

The present method for BPC detection is based on the well-known observation that a BPC causes a systematic shift of the electrical axis that reflects the main direction of the VCG loop (RIEKKINEN and RAUTAHARJU, 1976); a similar relationship has not been established between ischaemic episodes and axis shifts. The method exploits shifts in loop direction by assuming that a BPC is manifested by a certain 'signature' in the series of rotation angles that result from the alignment of successive loops to a reference loop. A Bayesian approach is then taken to the detection problem, and the performance of the resulting detector is studied on a database with ECG signals recorded during different types of BPC.

2 Methods

2.1 *BPC characterisation using rotation angles*

An observed VCG loop, represented by the matrix $\boldsymbol{Z}$, is assumed to derive from a reference loop $\boldsymbol{Z}_R$ but to be altered through certain geometrical transformations caused by changes in body position and other extracardiac sources. The time location of the loop is determined by QRS detection. As the terminal part of the QRS complex and the ST-T segment are most prone to ischaemia-induced changes in morphology, only the initial part of the QRS complex is used to define the VCG loop in this study; see Fig. 1. The alignment involves three transformations described by the scalar amplitude factor α, the rotation matrix $\boldsymbol{Q}$ and the time shift matrix $\boldsymbol{J}_\tau$. Estimates of these parameters are obtained by minimising the normalised Euclidean distance $\mathcal{E}$ between the samples of the two loops

$$\mathcal{E} = \frac{\|\boldsymbol{Z} - \alpha \boldsymbol{Q}\boldsymbol{Z}_R\boldsymbol{J}_\tau\|_F^2}{\|\alpha \boldsymbol{Q}\boldsymbol{Z}_R\boldsymbol{J}_\tau\|_F^2} \tag{1}$$

The Frobenius norm for an $N \times M$ matrix $\boldsymbol{X}$ is defined by

$$\|\boldsymbol{X}\|_F^2 = \sum_{i=1}^{M}\sum_{j=1}^{N} |x_{ij}|^2 \tag{2}$$

The matrices $\boldsymbol{Z}$ and $\boldsymbol{Z}_R$ have dimensions $3 \times N$ and $3 \times (N + 2\Delta)$, respectively, where the columns contain the orthogonal leads X, Y and Z. The 3×3 rotation matrix $\boldsymbol{Q}$ is orthonormal, i.e. $\boldsymbol{Q}\boldsymbol{Q}^T = \boldsymbol{I}$, where $\boldsymbol{I}$ denotes the unit matrix. The time shift matrix $\boldsymbol{J}_\tau$ is introduced to ensure that the two loops are temporally well-aligned; therefore $\boldsymbol{Z}_R$ is symmetrically augmented with 2Δ samples, such that different time intervals of $\boldsymbol{Z}_R$ can be selected and aligned to $\boldsymbol{Z}$. The matrix $\boldsymbol{J}_\tau$ is defined by the integer-valued time shift τ

$$\boldsymbol{J}_\tau = \begin{bmatrix} \boldsymbol{0}_{\Delta+\tau} \\ \boldsymbol{I} \\ \boldsymbol{0}_{\Delta-\tau} \end{bmatrix} \tag{3}$$

where $\tau = -\Delta, \ldots, \Delta$. The dimensions of the upper and lower zero matrices in (3) are equal to $(\Delta + \tau) \times N$ and $(\Delta - \tau) \times N$, respectively, and $\boldsymbol{I}$ is $N \times N$. The introduction of the normalised distance criterion in (1) is motivated by the observation that an unnormalised criterion, such as the one suggested in SÖRNMO (1998), results in temporal synchronisation that favours selection of the lower-amplitude interval (i.e. the PQ interval) of the two loops, as the smallest distance will occur in that interval. By normalising each selected interval with its energy, more reliable angle estimates are obtained, as the smallest distance instead will be found in an interval with a much higher signal-to-noise ratio (SNR). Thus the normalised criterion is particularly important to consider when only parts of the QRS complex are analysed.

The distance $\mathcal{E}$ is globally minimised by first finding the estimates of α and $\boldsymbol{Q}$ for every value of τ, and then selecting that τ (and related estimates of α and $\boldsymbol{Q}$) that minimises (1); the details of the minimisation can be found in Appendix 1. For a fixed value of τ, the optimum estimate of the rotation matrix is obtained by

$$\hat{\boldsymbol{Q}}_\tau = \boldsymbol{U}_\tau \boldsymbol{V}_\tau^T \tag{4}$$

where the matrices $\boldsymbol{U}_\tau$ and $\boldsymbol{V}_\tau$ result from singular value decomposition of the matrix $\boldsymbol{D}_\tau = \boldsymbol{Z}\boldsymbol{J}_\tau^T\boldsymbol{Z}_R^T$ containing the left and right singular vectors, respectively. Once $\hat{\boldsymbol{Q}}_\tau$ is available, an estimate of the scalar α is obtained by

$$\hat{\alpha}_\tau = \frac{\mathrm{tr}(\boldsymbol{Z}^T\boldsymbol{Z})}{\mathrm{tr}(\boldsymbol{Z}^T\hat{\boldsymbol{Q}}_\tau\boldsymbol{Z}_R\boldsymbol{J}_\tau)} \tag{5}$$

Finally, to find the minimum distance $\mathcal{E}_{min}$, the estimation procedure defined by (4) and (5) is repeated for all values of τ within the interval $-\Delta \le \tau \le \Delta$, and the value of τ yielding the minimum is selected

$$\hat{\tau} = \arg \min_{-\Delta \le \tau \le \Delta} \frac{\|\boldsymbol{Z} - \hat{\alpha}_\tau\hat{\boldsymbol{Q}}_\tau\boldsymbol{Z}_R\boldsymbol{J}_\tau\|_F^2}{\|\hat{\alpha}_\tau\hat{\boldsymbol{Q}}_\tau\boldsymbol{Z}_R\boldsymbol{J}_\tau\|_F^2} \tag{6}$$

Although the parameter α was not judged to be as useful for BPC detection as the rotation angles, scaling is still considered, as it may implicitly improve the accuracy of $\hat{\tau}$ in (6).

The optimum estimate $\hat{\boldsymbol{Q}}$ describes the rotation of the VCG loop. As such a rotation can be viewed as three successive rotations defined by the rotation angles φ_X, φ_Y and φ_Z, i.e.

$$\begin{aligned} \boldsymbol{Q} = &\begin{bmatrix} 1 & 0 & 0 \\ 0 & \cos\varphi_X & \sin\varphi_X \\ 0 & -\sin\varphi_X & \cos\varphi_X \end{bmatrix} \begin{bmatrix} \cos\varphi_Y & 0 & \sin\varphi_Y \\ 0 & 1 & 0 \\ -\sin\varphi_Y & 0 & \cos\varphi_Y \end{bmatrix} \\ &\times \begin{bmatrix} \cos\varphi_Z & \sin\varphi_Z & 0 \\ -\sin\varphi_Z & \cos\varphi_Z & 0 \\ 0 & 0 & 1 \end{bmatrix} \\ = &\begin{bmatrix} * & \sin\varphi_Z\cos\varphi_Y & \sin\varphi_Y \\ * & * & \sin\varphi_X\cos\varphi_Y \\ * & * & * \end{bmatrix} \end{aligned} \tag{7}$$

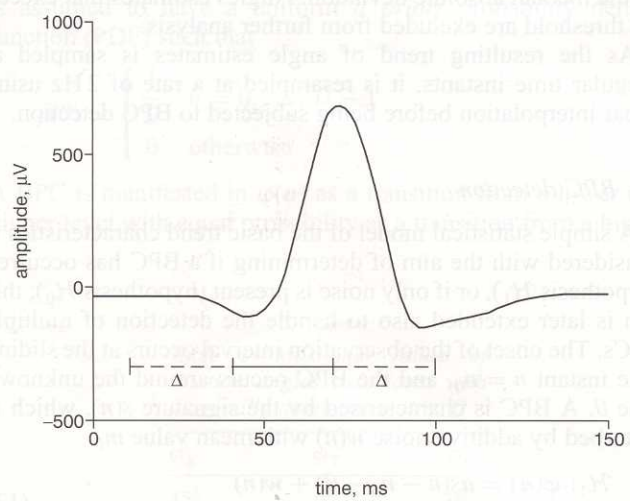

Fig. 1 *QRS complex and two time intervals used in loop alignment: interval always included and interval extended by Δ at each end*

estimates of these angles can be obtained by identifying the proper elements of $\hat{\boldsymbol{Q}}$ with those given in (7); the asterisk '*' denotes a 'don't care' matrix entry. The identification yields the following estimates:

$$\hat{\varphi}_2 = \hat{\varphi}_Y = \arcsin(\hat{q}_{13}) \tag{8}$$

$$\hat{\varphi}_1 = \hat{\varphi}_X = \arcsin\left(\frac{\hat{q}_{23}}{\cos\hat{\varphi}_Y}\right) \tag{9}$$

$$\hat{\varphi}_3 = \hat{\varphi}_Z = \arcsin\left(\frac{\hat{q}_{12}}{\cos\hat{\varphi}_Y}\right) \tag{10}$$

where $\hat{q}_{mn}$ denotes the element of the mth row and nth column of $\hat{\boldsymbol{Q}}$.

Although the loop alignment technique was developed for the processing of one loop at a time, it can easily be extended to the alignment of successive loops. In doing so, we obtain three series of rotation angle estimates, irregularly sampled at the time instants when the heart beats. Fig. 2 presents an example where the three angle series contain BPCs at the rate of one every minute. A series is typically composed of two different components: short-term oscillations, mainly due to respiratory activity (manifested as 'superimposed noise'), and abrupt step changes due to BPCs. During a BPC, the increased level of muscular noise further increases the level of short-term oscillations.

2.2 *Rotation matrix property*

A detailed study of the above alignment procedure revealed that large estimation errors occasionally were related to the computation of $\hat{\tau}$. For successive beats with similar morphologies, we can expect that changes in the direction of the electrical axis are relatively small, with angle fluctuations within $\pm 15°$ (ADAMS and DREW, 1997). Such a range of angles implies that the rotation matrix is diagonally dominant. However, at higher ECG noise levels, it was observed that $\hat{\boldsymbol{Q}}$ did not always possess such a structure, implying that the major part of one lead derives from the other two leads. By studying the estimates of $\boldsymbol{Q}$ for different values of τ, it was found that the rotation matrix became diagonally dominant for values adjacent to $\hat{\tau}$.

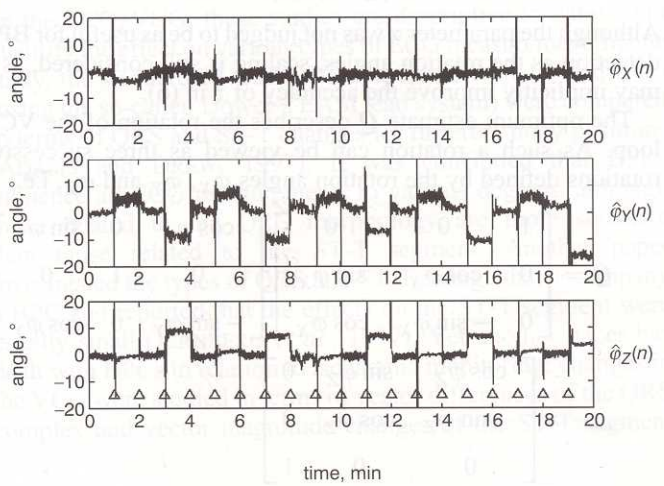

Fig. 2 *Example of estimated rotation angles $\hat{\varphi}_X(n)$, $\hat{\varphi}_Y(n)$ and $\hat{\varphi}_Z(n)$. Change in body position of subject occurs at onset of every minute (indicated by triangles)*

*Equipment from Siemens-Elema AB, Solna, Sweden

One technique that solves this particular problem is simply to discard those $\hat{\boldsymbol{Q}}_\tau$ that are not diagonally dominant and to evaluate the distance criterion based on the remaining set of matrices. A diagonally dominant matrix is here defined as

$$q_{nn,\tau}^2 > \sum_{\substack{m,n=1,2,3 \\ n\neq m}} q_{kl,t}^2 \quad n = 1, 2, 3 \tag{11}$$

where $-\Delta \leq \tau \leq \Delta$. The resulting set of diagonally dominant matrices is contained in the set denoted by Ω_τ. The final estimate $\check{\tau}$ is obtained by a constrained grid search defined by

$$\check{\tau} = \arg\min_{\tau\in\Omega_\tau} \frac{\|\boldsymbol{Z} - \hat{\alpha}_\tau \hat{\boldsymbol{Q}}_\tau \boldsymbol{Z}_R \boldsymbol{J}_\tau\|_F^2}{\|\hat{\alpha}_\tau \hat{\boldsymbol{Q}}_\tau \boldsymbol{Z}_R \boldsymbol{J}_\tau\|_F^2} \tag{12}$$

In the unlikely case of an empty set Ω_τ, the loop is simply excluded from further analysis.

The effect of introducing the constraint on diagonal dominance is illustrated by Fig. 3, where the combination of a high noise level and leads with similar morphologies were found to result in inaccurate angle estimates. From Fig. 3, it is evident that the modified alignment method in (12) produces a more accurate rotation, although it no longer yields the minimum $\mathcal{E}$. The theoretical limits for diagonal dominance are presented in Table 1 for the symmetrical cases with one, two and three identical rotation angles and with the remaining rotation angles set to zero. From this Table, it can be concluded that the maximum amount of rotation allowed by the diagonal constraint is well above what can be expected during a BPC (ADAMS and DREW, 1997).

2.3 *Noisy beat rejection and resampling*

As the angle estimates become unreliable in situations with poor SNR, two strategies for excluding such estimates are used: SNR-based rejection and outlier rejection. Based on an SNR measure involving the QRS amplitude and the noise level in the TQ interval, a beat is excluded whenever its SNR drops below an exponentially updated threshold based on earlier SNRs. This type of dynamic threshold is used to handle the fact that the SNR varies considerably during a BPC. It also makes it possible to eliminate noisy beats for a shorter period of time, while maintaining the long-term ability to detect a BPC at lower SNRs.

The SNR-based rejection is supplemented with a simple but effective method for outlier rejection, the so-called X84 rejection method (HAMPEL *et al.*, 1986). This method finds disproportionately large angle values by testing the difference between the angle estimates and the median against a threshold that depends on the median absolute deviation. Angles estimates that exceed the threshold are excluded from further analysis.

As the resulting trend of angle estimates is sampled at irregular time instants, it is resampled at a rate of 2 Hz using linear interpolation before being subjected to BPC detection.

2.4 *BPC detection*

A simple statistical model of the basic trend characteristics is considered with the aim of determining if a BPC has occurred (hypothesis $\mathcal{H}_1$), or if only noise is present (hypothesis $\mathcal{H}_0$); this aim is later extended also to handle the detection of multiple BPCs. The onset of the observation interval occurs at the sliding time instant $n = n_0$, and the BPC occurs around the unknown time θ. A BPC is characterised by the signature $s(n)$, which is disturbed by additive noise $\boldsymbol{w}(n)$ with mean value m_l

$$\begin{aligned} \mathcal{H}_1&: \boldsymbol{\varphi}(\boldsymbol{n}) = \boldsymbol{a}s(n - n_0 - \theta) + \boldsymbol{w}(n) \\ \mathcal{H}_0&: \boldsymbol{\varphi}(\boldsymbol{n}) = \boldsymbol{w}(n) \end{aligned} \tag{13}$$

for $n = n_0, \ldots, n_0 + M - 1$, where

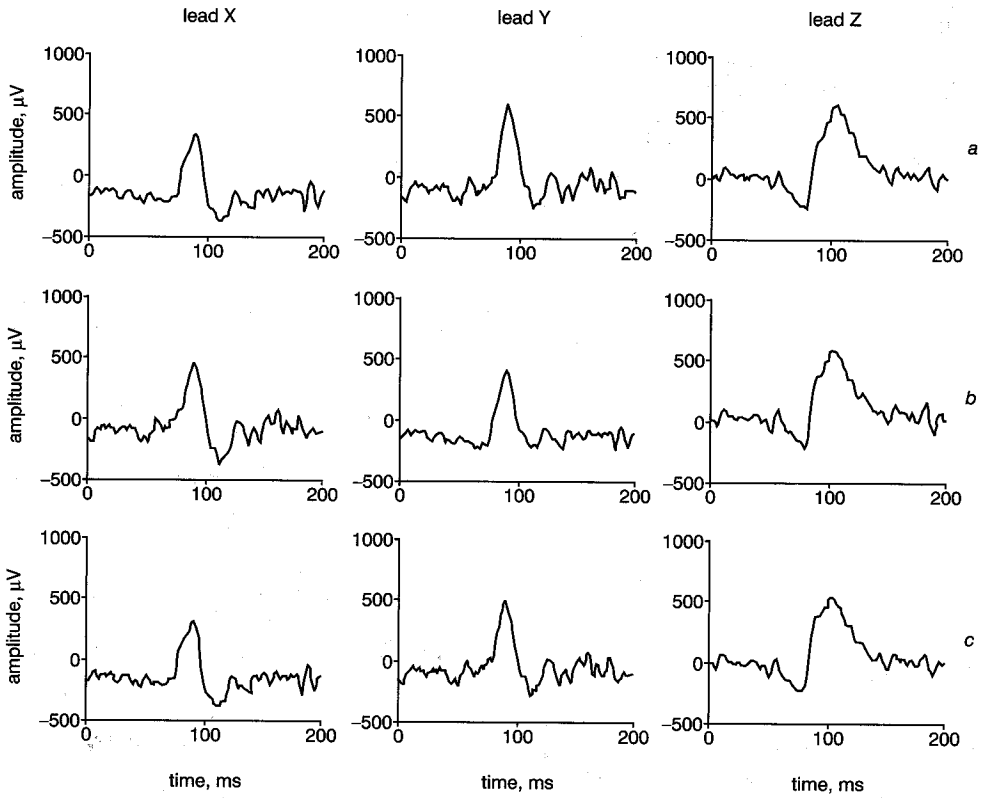

Fig. 3 *Effect of diagonally/non-diagonally dominant rotation matrix: (a) leads X, Y and Z of original VCG signal; (b) leads after rotation with optimum but non-diagonally dominant matrix; (c) leads after use of constrained loop alignment in (12), resulting in diagonally dominant matrix. Note that beat morphologies in (a) and (c) better resemble each other than those in (a) and (b), where S-wave in lead Y is almost lost*

$\boldsymbol{\varphi}(n) = [\varphi_1(n)\ \varphi_2(n)\varphi_3(n)]^T$, $\boldsymbol{w}(n)$ and $\boldsymbol{a}$ are 3×1 vectors representing information related to each of the orthogonal leads. For simplicity, it is assumed that $s(n)$ is modelled by a step changes

$$s(n) = \begin{cases} \dfrac{1}{\sqrt{D}} & n = 0, \ldots, \dfrac{D}{2} - 1 \\ -\dfrac{1}{\sqrt{D}} & n = \dfrac{D}{2}, \ldots, D - 1 \\ 0 & \text{otherwise} \end{cases} \tag{14}$$

where the length of $s(n)$ is defined by the even-valued integer D. The length M is chosen such that $s(n)$ is completely contained in the observation interval. The discrete-valued occurrence time θ is assumed to have a uniform *a priori* probability density function (PDF) such that

$$p(\theta) = \begin{cases} \dfrac{1}{D} & \theta = 0, \ldots, D - 1 \\ 0 & \text{otherwise} \end{cases} \tag{15}$$

A BPC is manifested in $\boldsymbol{\varphi}(n)$ as a transition from a lower to a higher level with equal probability as a transition from a higher to a lower level. Therefore the amplitude a_l is, in each lead, characterised by a 'two-point' *a priori* PDF

$$p(a_l) = \begin{cases} \dfrac{1}{2} & a_l = a_l^0 \\ \dfrac{1}{2} & a_l = -a_l^0 \end{cases} \tag{16}$$

where a_l^0 is a positive-valued constant representing the magnitude of the BPC. Hence, the magnitude of a transition in the lth lead has a fixed size equal to $2a_l^0$. The possible combinations of the amplitudes $\boldsymbol{a}$ that can occur are denoted by the set Ω_a. The additive noise is assumed to be white and Gaussian, with mean m_l and variance $\sigma_{w_l}^2$

$$p(\boldsymbol{W}(n_0)) = \prod_{n=n_0}^{n_0+M-1} \prod_{l=1}^{3} \frac{1}{\sqrt{2\pi}\sigma_{w_l}} \exp\left(-\frac{(w_l(n) - m_l)^2}{2\sigma_{w_l}^2} \right) \tag{17}$$

where $\boldsymbol{W}(n_0) = [\boldsymbol{w}(n_0) \cdots \boldsymbol{w}(n_0 + M - 1)]^T$. All random variables in θ, $\boldsymbol{a}$ and $\boldsymbol{W}(n_0)$ are assumed to be mutually independent.

A Bayesian approach is adopted for developing a BPC detector that takes its starting point in the binary detection problem with random, unwanted parameters, i.e. θ and $\boldsymbol{a}$ (VAN TREES, 1968; KAY, 1998). The two hypotheses are characterised by the PDFs $p(\Phi(n_0)|\theta, \boldsymbol{a}, \mathcal{H}_1)$, indicating that a BPC has occurred, and $p(\Phi(n_0)|\mathcal{H}_0)$, indicating that nothing has changed; the matrix $\Phi(n_0) = [\boldsymbol{\varphi}(n_0) \cdots \boldsymbol{\varphi}(n_0 + M - 1)]^T$

Table 1 Maximum values of rotation angles associated with diagonally dominant matrix $\boldsymbol{Q}$

φ_X	φ_Y	φ_Z
45°	0°	0°
32.8°	32.8°	0°
26.7°	26.7°	26.7°

contains all observations of the three leads. The Bayesian detector requires that the likelihood ratio is tested against a threshold η, such that hypothesis $\mathcal{H}_1$ is decided if

$$\Lambda(\Phi(n_0)) \stackrel{\text{def}}{=} \frac{p(\Phi(n_0)|\mathcal{H}_1)}{p(\Phi(n_0)|\mathcal{H}_0)} = \frac{\sum_{\Omega_a}\sum_{\theta} p(\Phi(n_0)|\theta, \boldsymbol{a}, \mathcal{H}_1)\ p(\theta, \boldsymbol{a})}{p(\Phi(n_0)|\mathcal{H}_0)} > \eta \quad (18)$$

where the two sums are introduced because the random variables θ and $\boldsymbol{a}$ are discrete-valued. The threshold is commonly treated as a design parameter and selected such that a certain performance is achieved, e.g. in terms of false alarm rate. The detector in (18) is rather demanding computationally, and therefore a simplified detector based on the Taylor series expansion has been derived; see Appendix 2. Assuming that the three leads have identical statistical properties, the simplified detector is defined by the sum of the energy of the matched filter output $y_l(n_0 + \theta)$ of all leads

$$\sum_{\theta=0}^{D-1}\sum_{l=1}^{3} y_l^2(n_0 + \theta) \geq \eta' \quad (19)$$

where the modified threshold η' is defined in Appendix 2.

To detect multiple BPCs, the detection test is repeated for successive values of n_0, until the entire signal has been processed. Hence, the detector performs a 'sliding' hypothesis test to find out whether a BPC has occurred or not. Once a BPC has been detected, the threshold test is inhibited for 10 s to ensure that a single BPC is not detected twice.

3 Database

The performance of the BPC detector was studied on an ECG database collected from 20 healthy subjects (nine females, 32 ± 9 years old). The subjects were instructed to change their body position in the following sequence: supine, right side, supine, left side, supine. Each position was held for 1 min, so that muscular activity and other artifacts were allowed to decay before the next BPC was initiated. The sequence was repeated five times so that the method's performance could be better assessed; thus, the total duration of each ECG recording was 20 min.

The standard 12-lead ECG was acquired at a sampling rate of 1 kHz and with an amplitude resolution of 0.6 μV. As the BPC detector requires a VCG signal, such a signal was synthesised from the 12-lead ECG using the inverse Dower method (MACFARLANE *et al.*, 1994).

4 Results

The performance of the BPC detector was evaluated in terms of the probability of missed detection P_M and the probability

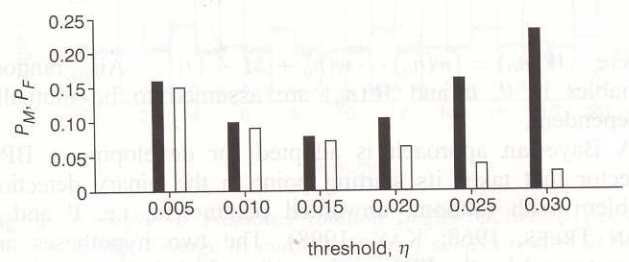

Fig. 4 *BPC detector performance in terms of (■) P_M and (□) P_F for different values of detection threshold η*

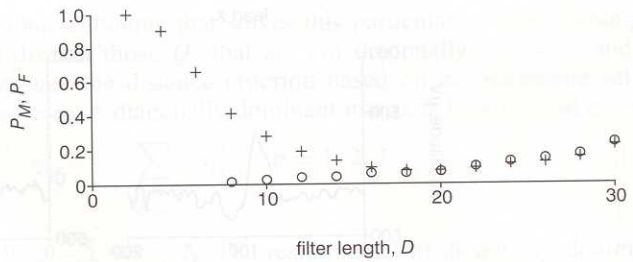

Fig. 5 *BPC detector performance, in terms of (+)P_M and (o)P_F, as function of signal length D. Results were obtained for $\eta' = 0.015$*

of false alarm P_F. These performance measures were estimated from the numbers of true detections N_T, false alarms N_F and missed detections N_M, such that $P_M = N_M/(N_T + N_M)$ and $P_F = N_F/(N_T + N_F)$. A BPC was considered as a true detection whenever the detector output was contained within a 20 s interval positioned around the BPC.

Fig. 4 presents the performance measures P_M and P_F for different values of the detection threshold η'. For values above 0.015, P_M deteriorates quite rapidly, whereas P_F slowly decreases. For η' values below 0.015, P_M no longer decreases but rather increases, owing to the fact that false alarms inhibit the detection of certain true BPCs. The results in Fig. 4 suggest that a good over-all detector performance is achieved when η' is chosen around 0.015. For $\eta' = 0.015$, the performance figures are $P_M = 0.08$ and $P_F = 0.07$.

The performance was also investigated for different signal lengths D; see (14). Fig. 5 shows that a length of 16–18 samples should be used to achieve a low P_M (corresponding to a filter delay of about 4 s for a resampling rate of 2 Hz). The increase in P_M observed for large values of D is due to the increased detection interval length which, again, inhibits certain BPCs from being detected; therefore D should preferably not exceed 20.

Fig. 6 presents an example in which two BPCs are missed. From the three series of angle estimates, no shifts can be observed at 3 min and 4 min, despite the fact that BPCs took place at these times (Figs 6*a–c*). As a result, no peaks can be discerned in the detection function, as defined in (19), at these times. Interestingly, Fig. 6*e* reveals that distinct changes in the amplitudes of three VCG leads take place at these times. The major difference between the second and the fourth minute is that, whereas the amplitudes of leads Y and Z increase during the second minute, the amplitude of lead X decreases. The effect of the amplitude changes can be interpreted as an axis shift in the angle estimates. During the fourth minute, on the other hand, the amplitudes of X and Y are both increased, whereas that of Z is essentially unchanged. Thus a BPC is, in this case, not reflected by a significant axis shift but rather by marked changes in the α series.

5 Discussion

Ischaemia monitoring is the target application of the present detector, although other applications may be of interest as well where BPC information is needed. In monitoring applications, the ischaemia detector polls the BPC detector only when a potential ischaemic event is detected. Accordingly, it is important that the BPC detector does not classify an ischaemic event as a BPC. On the other hand, false alarms of the BPC detector unrelated to ischaemic events can be more easily accepted, as these do not influence the performance of the ischaemia

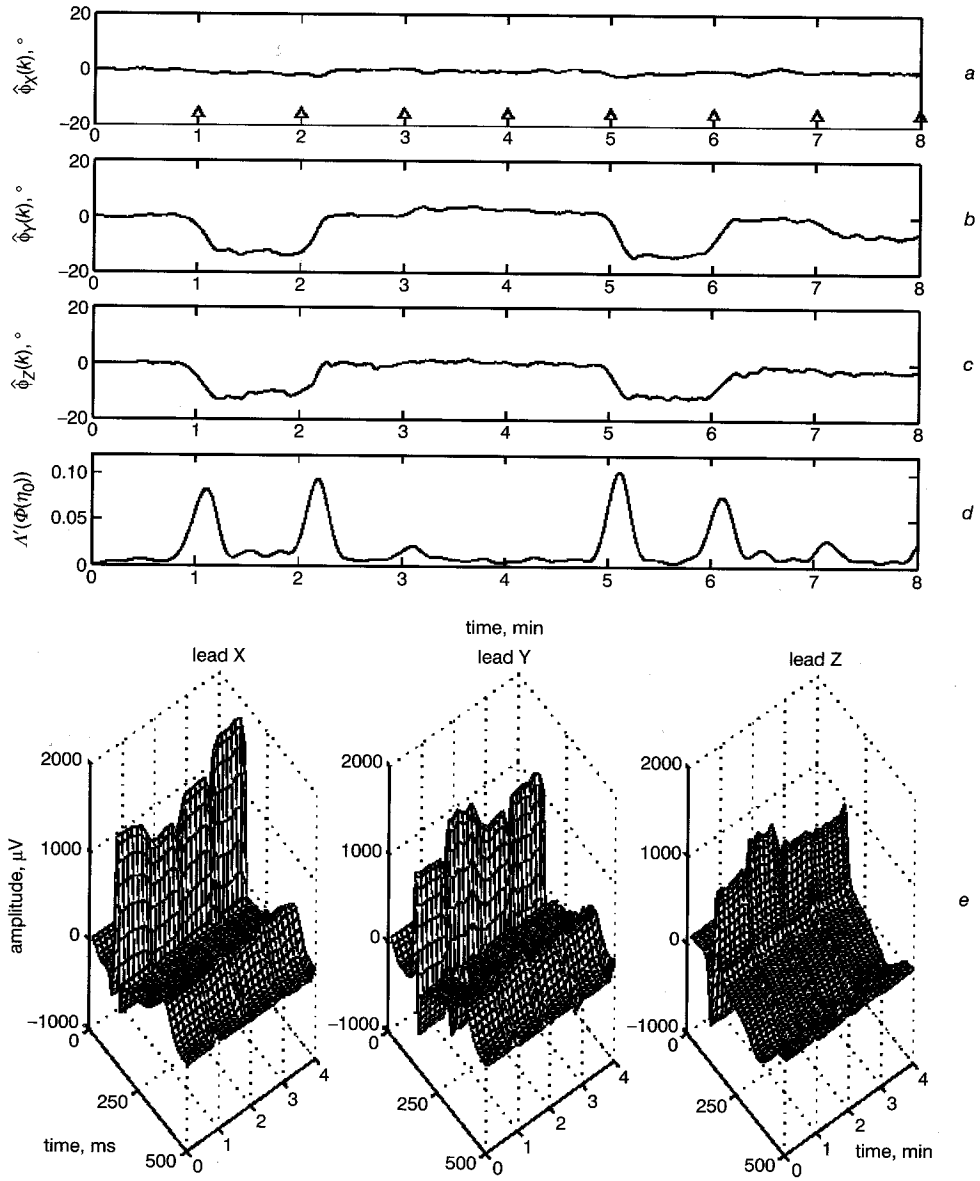

Fig. 6 *Example of missed BPCs. Rotation angles of (a) lead X (BPCs are indicated with triangles), (b) lead Y and (c) lead Z. (d) Detection function defined in (19). (e) Successive cardiac cycles of leads X, Y and Z during first 4 min of recording*

detector. In the rather unlikely case of a BPC missed by the BPC detector but found by the ischaemia detector, the cost associated with a BPC labelled as an ischaemic event is evidently less than that of an ischaemic event labelled as a BPC.

The detector is based on the well-known fact that a BPC causes a shift in the electrical axis of the heart. Such shifts are quantified by estimation of rotation angles using a newly proposed criterion for loop alignment. The introduction of the criterion in (1) is central to the present study and was motivated by initial, less successful efforts based on the unnormalised criterion. A number of additional techniques were introduced to reject unreliable angle estimates at poor SNRs, as an earlier study showed that loop alignment performance can deteriorate considerably at such SNRs (ÅSTRÖM *et al.*, 2000).

The BPC detector is based on a simple model of the BPC signature and the related likelihood ratio test, albeit in a simplified form. Various shapes of $s(n)$ were investigated but were found to have negligible influence on performance. The Taylor approximation introduced in the detection test is not valid for high SNRs, however, the simplified detector will, for such SNRs, result in an acceptable detection rate, as the separation between the two hypotheses remains good. The resulting, simplified detector is attractive, not only from a computational viewpoint, but because the Taylor approximation leads to a detector where neither estimates of the signal amplitude a_l^0 nor as the noise mean m_l nor variance $\sigma_{w_l}^2$ are required.

Future improvements should include better handling of cases where a BPC is primarily manifested as a change in α; see Fig. 6. Such an improvement is likely to reduce the number of missed BPCs. The ECG noise level is another quantity that could be incorporated in the detector, as a BPC is typically associated with an increase in this level; preliminary results indicate that such information improves the performance.

The main purpose of this paper has been to describe a new methodology for BPC detection and to indicate its performance on a database with BPCs only. In a recent study, we have compared the performance of a method based on the Karhunen–Loève transform to that of the above detector, using a database containing ischaemic events recorded during percutaneous transluminal coronary angiography, but without the presence of BPCs (GARCIA *et al.*, 2003); the results of that study gave an indication of the number of false positives produced by the

detectors. However, the over-all value of a method can only be fully assessed once the performance on a database containing both ischaemic episodes and BPCs has been investigated. The formation of such a database is associated with considerable efforts and was not feasible to undertake within the present study.

The comprehensive efforts by Jager and colleagues (see, for example, JAGER *et al.* (1996; 2000)) have recently resulted in the availability of a database (LTST-DB) that is very well suited for the development and performance evaluation of BPC detection algorithms. The database consists of 80 24 h, three-lead ECG recordings that have been annotated with respect to, for example, the presence of transient ischaemic events and non-ischaemic ST events due to axis shifts.

Acknowledgments—This work was supported in part by grants from the Swedish National Board for Technical Development (VINNOVA) and CICYT (TIC2001-2167-CO2-02), and DGA P075-2001 Spain.

Appendix 1

Estimation of loop alignment parameters

The minimisation of (1) is achieved by rewriting it as

$$\mathcal{E} = \frac{\mathrm{tr}(\boldsymbol{Z}^T\boldsymbol{Z}) + \alpha^2\mathrm{tr}(\boldsymbol{J}_\tau^T\boldsymbol{Z}_R^T\boldsymbol{Z}_R\boldsymbol{J}_\tau) - 2\alpha\mathrm{tr}(\boldsymbol{Z}^T\boldsymbol{Q}\boldsymbol{Z}_R\boldsymbol{J}_\tau)}{\alpha^2\mathrm{tr}(\boldsymbol{J}_\tau^T\boldsymbol{Z}_R^T\boldsymbol{Z}_R\boldsymbol{J}_\tau)}$$

and noting that minimisation with respect to $\boldsymbol{Q}$ is equivalent to maximising the rightmost term in the numerator, as the other terms are independent of $\boldsymbol{Q}$. It is possible first to determine $\hat{\boldsymbol{Q}}_\tau$ independently of $\hat{\alpha}_\tau$ by means of the temporary matrix $\boldsymbol{D}_\tau = \boldsymbol{Z}\boldsymbol{J}_\tau^T\boldsymbol{Z}_R^T$. Singular value decomposition of $\boldsymbol{D}_\tau$ (SÖRNMO, 1998)

$$\boldsymbol{D}_\tau = \boldsymbol{U}_\tau\Sigma_\tau\boldsymbol{V}_\tau^T$$

yields the optimum $\hat{\boldsymbol{Q}}_\tau$ as

$$\hat{\boldsymbol{Q}}_\tau^T = \boldsymbol{U}_\tau\boldsymbol{V}_\tau^T$$

where $\boldsymbol{U}_\tau$ and $\boldsymbol{V}_\tau$ denote the matrix with the left and right singular vectors, respectively. The matrix Σ_τ contains the singular values. The parameter α is estimated by differentiating $\mathcal{E}$ with respect to α

$$\frac{\partial\mathcal{E}}{\partial\alpha} = -2\alpha^{-3}\frac{\mathrm{tr}(\boldsymbol{Z}^T\boldsymbol{Z})}{\mathrm{tr}(\boldsymbol{J}_\tau^T\boldsymbol{Z}_R^T\boldsymbol{Z}_R\boldsymbol{J}_\tau)} + \alpha^{-2}\frac{2\mathrm{tr}(\boldsymbol{Z}^T\hat{\boldsymbol{Q}}_\tau\boldsymbol{Z}_R\boldsymbol{J}_\tau)}{\mathrm{tr}(\boldsymbol{J}_\tau^T\boldsymbol{Z}_R^T\boldsymbol{Z}_R\boldsymbol{J}_\tau)}$$

Setting this expression to zero gives $\hat{\alpha}_\tau$

$$\hat{\alpha}_\tau = \frac{\mathrm{tr}(\boldsymbol{Z}^T\boldsymbol{Z})}{\mathrm{tr}(\boldsymbol{Z}^T\hat{\boldsymbol{Q}}_\tau\boldsymbol{Z}_R\boldsymbol{J}_\tau)}$$

Finally, the estimation of τ is given by

$$\hat{\tau} = \arg\min_{-\Delta\le\tau\le\Delta}\frac{\|\boldsymbol{Z} - \hat{\alpha}_\tau\hat{\boldsymbol{Q}}_\tau\boldsymbol{Z}_R\boldsymbol{J}_\tau\|_F^2}{\|\hat{\alpha}_\tau\hat{\boldsymbol{Q}}_\tau\boldsymbol{Z}_R\boldsymbol{J}_\tau\|_F^2}$$

Appendix 2

Detector derivation

Introducing the definitions of the *a priori* PDFs of θ and $\boldsymbol{a}$ and the Gaussian noise assumptions, the likelihood ratio in (18) becomes

$$\Lambda(\Phi(n_0)) = \frac{1/8D\sum_{\theta=0}^{D-1}\sum_{i=1}^{2}\prod_{l=1}^{3}\prod_{n=n_0}^{n_0+M-1}\exp\left(-(\varphi_l(n) - m_l - (-1)^i \times a_l^0 s(n-n_0-\theta))^2/2\sigma_{w_l}^2\right)}{\prod_{l=1}^{3}\prod_{n=n_0}^{n_0+M-1}\exp\left(-(\varphi_l(n)-m_l)^2/2\sigma_{w_l}^2\right)}$$

This expression can be rewritten to display more clearly the influence of various factors

$$\Lambda(\Phi(n_0)) = \frac{1}{8D}\sum_{\theta=0}^{D-1}\prod_{l=1}^{3}e_l(\theta)\left[\exp\left(\frac{a_l^0}{\sigma_{w_l}^2}\times\sum_{n=n_0}^{n_0+M-1}(\varphi_l(n)-m_l)s(n-n_0-\theta)\right) + \exp\left(-\frac{a_l^0}{\sigma_{w_l}^2}\sum_{n=n_0}^{n_0+M-1}(\varphi_l(n)-m_l)\times s(n-n_0-\theta)\right)\right] \quad (20)$$

where

$$e_l(\theta) = \exp\left(-\frac{(a_l^0)^2}{2\sigma_{w_l}^2}\sum_{n=n_0}^{n_0+M-1}s^2(n-n_0-\theta)\right)$$

A further simplification of (20) can be achieved by noting that $s(n)$ is completely contained in the observation interval, and therefore the signal energy

$$E_s = \sum_{n=n_0}^{n_0+M-1}s^2(n-n_0-\theta) = 1$$

is one for all values of n_0 and θ, i.e.

$$\prod_{l=1}^{3}e_l(\theta) = \prod_{l=1}^{3}\exp\left(-\frac{(a_l^0)^2}{2\sigma_{w_l}^2}\right) = e_0$$

It is well known that the expressions in the exponents of (20) can be interpreted as a matched filter operation, where the impulse response is given by the time-reversed signal $h(k) = s(-k)$. Accordingly, the output signal of the matched filter $y_l(n_0+\theta)$ is given by

$$y_l(n_0+\theta) = \sum_{n=n_0}^{n_0+M-1}(\varphi_l(n)-m_l)h(\theta-n) = \sum_{n=n_0}^{n_0+M-1}\varphi_l(n)h(\theta-n)$$

where the second equality is due to the fact that $s(n)$ is an antisymmetric waveform. Consequently, it is not necessary to know the values of m_l. Making use of $y_l(n_0+\theta)$, the following expression of the likelihood function is obtained:

$$\Lambda(\Phi(n_0)) = \frac{e_0}{8D}\sum_{\theta=0}^{D-1}\left[\exp\left(\sum_{l=1}^{3}\frac{a_l^0}{\sigma_{w_l}^2}y_l(n_0+\theta)\right) + \exp\left(-\sum_{l=1}^{3}\frac{a_l^0}{\sigma_{w_l}^2}y_l(n_0+\theta)\right)\right] \quad (21)$$

The detector defined in (21) requires that the exponential of the matched filter output is computed before the threshold test can be applied. To simplify this procedure, an approximate structure is suggested, based on a truncated Taylor expansion of the exponential function

$$e^x = \sum_{i=0}^{\infty}\frac{x^i}{i!} \approx 1 + x + \frac{x^2}{2} \quad (22)$$

This approximation is only valid for $|x| \ll 1$, and therefore the SNR $(a_l^0)^2/\sigma_{w_l}^2$ in (21) is assumed to be less than one. Using this approximation, the likelihood function in (21) becomes

$$\Lambda'(\Phi(n_0)) = \frac{e_0}{8D}\sum_{\theta=0}^{D-1}\left(2 + \sum_{l=1}^{3}\frac{(a_l^0)^2}{\sigma_{w_l}^4}y_l^2(n_0+\theta)\right)$$

Assuming that a_l^0 and $\sigma_{w_l}^2$ are lead-independent, i.e. $a_l^0 \equiv a^0$ and $\sigma_{w_l}^2 \equiv \sigma_w^2$, this expression becomes

$$\Lambda'(\Phi(n_0)) = \frac{e_0}{4} + \frac{e_0(a^0)^2}{8D\sigma_w^4}\sum_{\theta=0}^{D-1}\sum_{l=1}^{3}y_l^2(n_0+\theta) > \eta$$

and is related to the weak signal detector described in HELSTROM (1995). If we incorporate all terms that do not depend on the data into the threshold η', a BPC is detected whenever

$$\sum_{\theta=0}^{D-1}\sum_{l=1}^{3}y_l^2(n_0+\theta) > \eta'$$

where

$$\eta' = \frac{8D\sigma_w^4}{e_0(a^0)^2}\left(\eta - \frac{e_0}{4}\right) \quad (23)$$

It may be of interest that the simplest possible Taylor series approximation, making use of only $(1+x)$ in (22), results in a meaningless detector, as (21) becomes identical to zero. Thus at least three terms must be included in the approximation. Furthermore, an approximation that includes terms with order higher than two implies that the SNR no longer can be incorporated in the threshold but must be estimated prior to the computation of $\Lambda'(\Phi(n_0))$.

References

ADAMS, M., and DREW, B. (1997): 'Body position effects on the electrocardiogram: implications for ischemia monitoring', *J. Electrocardiol.*, **30**, pp. 285–291

AMINIAM, K., ROBERT, P., BUCHSER, E. E., RUTSCHMANN, B., HAYOZ, D., and DEPAIRON, M. (1999): 'Physical activity monitoring based on accelerometry: validation and comparison with video observation' *Med. Biol. Eng. Comput.*, **37**, pp. 304–308

ASTRÖM, M., CARRO, E., SÖRNMO, L., LAGUNA, P., and WOHLFART, B. (2000): 'Vectorcardiographic loop alignment and the measurement of morphologic beat-to-beat variability in noisy signals', *IEEE Trans. Biomed. Eng.*, **47**, pp. 497–506

DREW, B., and ADAMS, M. (2001): 'Clinical consequences of ST-segment changes caused by body position mimicking transient myocardial ischemia: hazards of ST-segment monitoring?' *J. Electrocardiol.*, **34**, pp. 261–264

FOERSTER, F., SMEJA, M., and FAHRENBERG, J. (1999): 'Detection of posture and motion by accelerometry: a validation in ambulatory monitoring', *Comput. Human Behav.*, **15**, pp. 571–583

GARCIA, J., ÅSTRÖM, M., MENDIVE, J., LAGUNA, P., and SÖRNMO, L. (2003): 'ECG based detection of body position changes in ischemia monitoring', *IEEE Trans. Biomed. Eng.*, **50**, (accepted for publication)

HAMPEL, F., RONCHETTI, E., ROUSSEEUW, P., and STAHEL, W. (1986): 'Robust statistics' (John Wiley & Sons, New York, 1986)

HELSTROM, C. W. (1995): 'Elements of signal detection and estimation' (Prentice-Hall, Englewood Cliffs, USA, 1995)

JAGER, F., MOODY, G. B., TADDEI, A., ANTOLIČ, G., ZABUKOVEC, M., ŠKRJANC, M., EMDIN, M., and MARK, R. G. (1996): 'Development of a long term database for assessing the performance of transient ischemia detectors', *Comput. Cardiol.*, **23**, pp. 481–484

JAGER, F., TADDEI, A., EMDIN, M., ANTOLIČ, G., DORN, R., MOODY, G. B., GLAVIĆ, B., SMRDEL, A., VARANINI, M., ZABUKOVEC, M., BORDIGIAGO, S., MARCHESI, C., and MARK, R. G. (2000): 'The long-term ST database: a research resource for algorithm development and physiologic studies of transient myocardial ischemia', *Comput. Cardiol.*, **27**, pp. 841–844

JAGER, F. J., MOODY, G. B., and MARK, R. G. (1998): 'Detection of transient ST segment episodes during ambulatory EGG monitoring' *Comput. Biomed. Res.*, **31**, pp. 305–322

JENSEN, S. M., HÄGGMARK, S., JOHANSSON, G., and NÄSLUND, U. (1997): 'On-line computerized vectorcardiography: influence of body position, heart rate, radiographic contrast fluid and myocardial ischemia', *Cardiol.*, **88**, pp. 576–584

JERNBERG, T., LINDAHL, B., HÖGBERG, M., and WALLENTIN, L. (1997): Effects on QRS-waveforms and ST-T-segment by changes in body position during continuous 12-lead EGG: A preliminary report, *Comput. Cardiol.*, **24**, pp. 461–464

KAY, S. M. (1998): 'Fundamentals of statistical signal processing—detection theory' (Prentice-Hall, New Jersey, 1998)

MACFARLANE, P., EDENBRANDT, L., and PAHLM, O. (1994): '12-lead vectorcardiography' (Butterworth-Heinemann, Oxford, 1994)

NELWAN, S. P., MEIJ, S. H., VAN DAM, T., and KLOOTWIJK, P. (2000): 'Detection of body position changes and its effect on ST-changes in the continuous 12-lead electrocardiogram', *Comput. Cardiol.*, **27**, pp. 825–828

NG, J., SAHAKIAN, A. V., and SWIRYN, S. (2000): 'Sensing and documentation of body position during ambulatory ECG monitoring', *Comput. Cardiol.*, **27**, pp. 77–80

NØRGAARD, B., RASMUSSEN, B., DELLBORG, M., and THYGESEN, K. (2000): 'Positional changes of spatial QRS- and ST-segment variables in normal subjects: implications for continuous vectorcardiography monitoring during myocardial ischemia', *J. Electrocardiol.*, **33**, 23–30

RIEKKINEN, H. and RAUTAHARJU, P. (1976): 'Body position, electrode level and respiration effects on the Frank lead electrocardiogram', *Circulation*, **53**, 40–45

SÖRNMO, L. (1998): 'Vectorcardiographic loop alignment and morphologic beat-to-beat variability', *IEEE Trans. Biomed. Eng.*, **45**, pp. 1401–1413

VAN TREES, H. L. (1968): 'Detection, estimation and modulation theory, Part I' (J. Wiley & Sons, New York, 1968)

Author's biography

MAGNUS ÅSTRÖM received his MSc in electrical engineering in 1997 from Lund University, Lund, Sweden, and is currently finishing his studies for the PhD in signal processing at the Department of Electroscience, Lund University. His research interests include signal processing techniques applied to cardiac electrical signals. A specific interest, is very low power signal processing algorithms for hardware implementation aimed for implantable devices such as pacemakers and defibrillators. Mr Åström has acted as a student representative of the department board since 1998.

Derivation errors in Appendix 2

May 14, 2004

In the paper:

Åmström M., García J., Laguna P., Pahlm O., y Sörnmo L. (2003). Detection of body position changes using the surface Electrocardiogram. *Medical and Biological Engineering and Computing*, vol. **41**, n. 2, pp. 164-171.

It have been identified two derivation error in Appendix 2, that even not affecting the final result are listed here for completeness of the work.

1 Error in equation (20) of Appendix 2

Equation (20) in appendix 2 should be

$$\Delta(\Phi(n_0)) = \frac{1}{8D}\sum_{\theta=0}^{D-1}\prod_{k=1}^{3}e_k(\theta)\left[\prod_{l=1}^{3}\exp\left(\frac{a_l^0}{\sigma_{w_l}^2}\sum_{n=n_0}^{n_0+M-1}(\varphi_l(n)-m_l)s(n-n_0-\theta)\right)\right.$$
$$\left.+\prod_{l=1}^{3}\exp\left(-\frac{a_l^0}{\sigma_{w_l}^2}\sum_{n=n_0}^{n_0+M-1}(\varphi_l(n)-m_l)s(n-n_0-\theta)\right)\right]$$

2 Error in equation with no number previous to equation (21) of Appendix 2

It should be written like

$$\begin{aligned} y_l(n_0+\theta) &= \sum_{n=n_0}^{n_0+M-1}(\varphi_l(n)-m_l)h(\theta-n+n_0) \\ &= \sum_{n=n_0}^{n_0+M-1}\varphi_l(n)h(\theta-n+n_0) \end{aligned}$$

Acknowledgement: Thanks to Ana Mincholé that point out this error